Delocalized and localized states of e$_g$ electrons in half-doped manganites

Delocalized and localized states of e$_g$ electrons in half-doped manganites

E L Winkler, M Tovar and M T Causa

Centro Atómico Bariloche, 8400 S C de Bariloche, RN, Argentina

E-mail: winkler@cab.cnea.gov.ar

Abstract

We have studied the magnetic behaviour of half-doped manganite $Y_{0.5}Ca_{0.5}MnO_3$ in an extended range of temperatures by means of magnetic susceptibility, $\chi(T)$, and electron spin resonance (ESR) experiments. At high temperature the system crystallizes in an orthorhombic structure. The resistivity value, $\rho \simeq 0.05\ \Omega$ cm at 500 K, indicates a metallic behaviour, while the Curie–Weiss dependence of $\chi(T)$ and the thermal evolution of the ESR parameters are very well described by a model that considers a system conformed by localized Mn^{4+} cores, t_{2g}^3, and itinerant, e$_g$, electrons. The strong coupling between t$_{2g}$ and e$_g$ electrons results in an enhanced Curie constant and an FM Curie–Weiss temperature that overcomes the AFM interactions between the t_{2g}^3 cores. A transition to a more distorted phase is observed at $T \approx 500$ K and signatures of localization of the e$_g$ electrons appear in the $\chi(T)$ behaviour below 300 K. A new Curie–Weiss regime is observed, where the Curie-constant value is consistent with dimer formation. Based on mean-field calculations, the dimer formation is predicted as a function of the interaction strength between the t$_{2g}$ and e$_g$ electrons.

(Some figures may appear in colour only in the online journal)

1. Motivation

The relationships between crystallographic structures, magnetic ordering, and electric properties of mixed valence manganites has been the subject of debate by experimental and theoretical researchers in the last 50 years. More recently new and interesting properties have been found. We are interested in half-doped manganites $L_{0.5}A_{0.5}MnO_3$, where L and A are 3+ and 2+ ions, respectively, and the Mn sites are equally occupied by Mn^{3+} ($3d^4$:$t_{2g}^3 e_g^1$) and Mn^{4+} ($3d^3$:$t_{2g}^3 e_g^0$) in a fully ionic picture.

The magnetic properties observed at low temperature for $La_{0.5}Ca_{0.5}MnO_3$ were firstly explained by Goodenough [1] in terms of a CE (striped) phase. In this model, charge ordering of localized Mn^{3+} and Mn^{4+} ions is proposed. In addition, orbital ordering, allowed by Jahn–Teller distortions of the O^{2-} octahedra, is also assumed. This particular structure is combined with Heisenberg superexchange interactions to give ferromagnetic (FM) zigzag spin chains interacting antiferromagnetically (AFM) with each other. More recently, a thorough study [2] of $L_{0.5}A_{0.5}MnO_3$ with L = lanthanides

or Y, and A = alkaline-earths showed that the low temperature magnetic order is strongly dependent on the lattice distortions quantified through the tolerance factor, t. The crossover from localized-electron (low t) to itinerant-electron (high t) behaviour is found at a critical value, $t_c \cong 0.975$.

Recent high resolution neutron diffraction in $Pr_{0.6}Ca_{0.4}MnO_3$ [3], $Pr_{0.5}Ca_{0.5}MnO_3$ [4], and $La_{0.5}Ca_{0.5}MnO_3$ [5] do not support the fully charge ordering structure in these compounds. Instead, a much smaller disproportionation, with $Mn^{3.5+\delta}/Mn^{3.5-\delta}$ ($\delta < 0.25$), gives a better description of the data. The observed low temperature magnetic structure [3] was then explained in terms of Mn dimers or Zener polarons (ZP) as elementary magnetic units that trap the e$_g$ electron and involve local distortions. The ZP structure is also the basis of the theoretical studies of Giovanetti *et al* [6], who predict the existence of magnetically induced multiferroic behaviour in half-doped manganites associated with the presence of Mn sites where the symmetry is broken. Aliaga *et al* [7] discuss the formation of this kind of cluster (FM islands of two to four Mn sites), through Monte-Carlo calculations in an FM Kondo lattice model that includes AFM interactions

between localized spins and FM double-exchange mediated by mobile—within the island—e_g electrons [8].

In the aforementioned paper [2], Rivadulla *et al* have suggested that there may be two different CE-type AFM insulating phases, one of them described by complete charge order ($t \leq 0.972$) and the other one based on the ordering of Mn dimers ($t \approx 0.980$). Additionally, different experiments, such as soft x-ray resonant diffraction [9], electron field gradient measurements [10], and solid state NMR ^{17}O spectrometry [11], show results that lead us to conclude that the occurrence of ZP phases in manganites with broken Mn-site symmetries remains a controversial issue.

Magnetic susceptibility $\chi(T)$ measurements are expected to reveal the formation of ZP even in the paramagnetic (PM) phase. Effectively, in the case of $Y_{0.5}Ca_{0.5}MnO_3$, Daoud *et al* [3] have determined a large effective moment, compatible with dimers, for $T < 220$ K. Measurements performed in $YBaMn_2O_6$ [12] reflect the presence of quatrimers (4-Mn clusters) below 480 K. These experiments allow the determination of characteristic temperatures for ZP formation since, at these temperatures, clearly visible anomalies [3, 12–14] are observed in the curves of $\chi(T)$ versus T. For higher temperatures, a FM Curie–Weiss behaviour is observed. Although the reported [3, 12, 13] effective moment seems to correspond at first sight to a mixture of ionic Mn^{3+} and Mn^{4+} resistivity measurements, [15] indicate that the system becomes metallic in this range of T, evidencing the mobility of the e_g electrons. This result is in agreement with the theoretical analysis of Aliaga [16] which predicts total delocalization of the e_g electrons at high temperature, accompanied by an important augmentation of the electrical conductivity.

In this paper we focus on the $Y_{0.5}Ca_{0.5}MnO_3$ half-doped manganite. We have extended the magnetic susceptibility experiments up to 1100 K in order to obtain a well characterized magnetic behaviour in the high temperature metallic state. We have also measured the temperature dependence of the ESR spectra and we have analysed it in terms of Bloch–Hasegawa equations, appropriate for a system of coupled localized moments (Mn^{4+}) and itinerant e_g electrons. Besides, using both magnetic susceptibility and ESR measurements, we have followed the process of cluster formation when the temperature diminishes.

2. Sample description and experimental details

The $Y_{0.5}Ca_{0.5}MnO_3$ perovskite samples were prepared by solid state reaction [17, 18] and analysed by x-ray diffraction between 20 and 750 K, see figure 1. The material is orthorhombic *Pnma* over this entire T range. At low temperatures, the three cell parameters are approximately constant and $b/\sqrt{2} < c < a$. Above 300 K the b parameter shows important variations and at the highest temperatures the system becomes more symmetric: a transition from a O$^{'}$-phase ($b/\sqrt{2} < c$) to an O-phase ($b/\sqrt{2} > c$) is observed at $T_S \approx 500$ K, see figure 1.

Magnetization (M) measurements were performed in the range 5–1100 K using SQUID ($T < 300$ K) and Faraday-balance ($T > 300$ K) magnetometers. High temperature
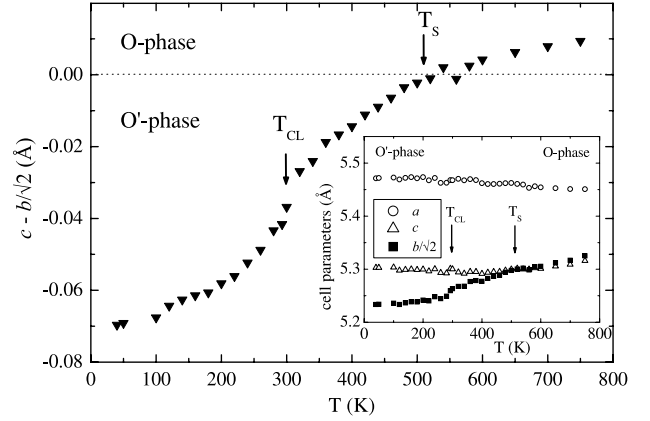

Figure 1. Cell parameters as a function of T (inset). Transition between O and O$^{'}$ phases at $T = T_S$ determined by the dependence $(c - b/\sqrt{2})(T)$ versus T.

measurements were made in a magnetic field $H \leq 5$ kOe; a linear behaviour was observed and the dc-magnetic susceptibility, $\chi(T)$, was derived. At low temperature the measurements were extended up to $H = 50$ kOe. ESR spectra were recorded with a Bruker ESP300 spectrometer operating at $\nu \approx 9.5$ GHz and equipped with special cavities to cover the temperature range from 2 to 800 K. From the ESR spectra in the paramagnetic regime, we determined three parameters: the resonance field (H_r), the linewidth (ΔH), and the ESR intensity (I_{ESR}). From H_r the factor $g = g_0 + \varepsilon$ was derived, where $g_0 = 2.0023$ corresponds to a free-electron and the g-shift, ε, depends on the nature of the 3d ion [19]. The effects of internal fields at low temperature, associated with the proximity of magnetic ordering, are responsible of changes in the g-factor, $g(T)$. The linewidth is a measurement of the spin relaxation mechanism and, in this work, it will be derived from the Bloch–Hasegawa phenomenological equations, see section 4 [19, 20]. From the derivative ESR absorption spectrum, ΔH is measured as the distance between its peaks. When ΔH and H_r have comparable magnitudes the contribution of the resonance centred at negative fields should be considered in order to obtain true values for the parameters [21]. The spectrum intensity could be determined from the area under the absorption curve (i.e. the double integral of the experimental curve), and should be proportional to the dc-susceptibility when all the magnetic ions contribute to the resonance.

3. Magnetization

In figure 2 we show $\chi^{-1}(T)$ versus T. The observed general behaviour is in accordance with previous measurements [3, 14] performed in a smaller range of T ($T \lesssim 700$ K) and with the findings in other half-doped manganites [12]. For $500 \leq T \leq 1100$ K the T-dependence shows a Curie–Weiss (CW)-like behaviour with Curie-constant $C_{HT} = 3.4(3)$ cm^3 K mol^{-1}, which corresponds to an effective magnetic moment $\mu_{eff} = 5.21$ μ_B and CW-temperature $\Theta_{HT} = 100(5)$ K.
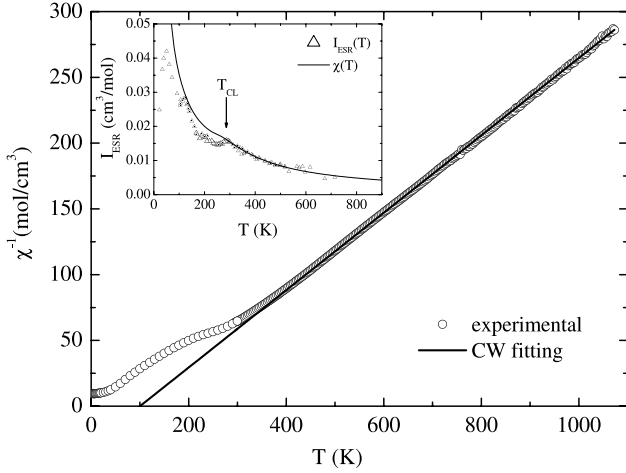
Figure 2. $\chi^{-1}(T)$ versus T: circles—experimental data; line—high temperature Curie–Weiss behaviour; inset: $I_{ESR}(T)$ versus T compared with $\chi(T)$.

In a fully ionic picture, the Mn sites in the $Y_{0.5}Ca_{0.5}MnO_3$ perovskite would be equally occupied by Mn^{3+} ($3d^4$:$t_{2g}^3e_g^1$) and Mn^{4+} ($3d^3$:$t_{2g}^3e_g^0$), with localized magnetic moments $\mu \simeq 4.90\ \mu_B$ and $3.87\ \mu_B$, respectively. Materials having non-equivalent magnetic sublattices and/or atoms are usually called ferrimagnetic [22] and a theoretical description of these systems was first made by Néel [23]. His prediction for the paramagnetic phase indicates that $\chi^{-1}(T)$ should asymptotically approach a CW law with a Curie constant given by the sample average: $C = [C_{Mn^{3+}} + C_{Mn^{4+}}]/2 = 2.4\ cm^3\ K\ mol^{-1}$. Notice that our determination for C_{HT} is significantly larger than that expected for the ionic picture. The CW temperature, in turn, should reflect an appropriate average of the magnetic interactions and at low T a hyperbolic behaviour for $\chi^{-1}(T)$ with negative curvature is expected. The positive value determined for Θ_{HT} indicates that FM interactions are dominant, but no signatures of ferrimagnetism are visible in figure 2. This result is consistent with studies [24, 25] on the series $Y_{1-x}Ca_xMnO_3$ that show ferrimagnetic behaviour only when $x < 0.2$ and $x > 0.8$, the ranges of small hole and electron doping levels.

On the other hand, strong FM interactions are often observed in mixed manganites, originated in the double-exchange mechanism mediated by itinerant electrons. In this picture, the magnetic lattice is conformed by localized (t_{2g}^3) electrons with total magnetic moment μ_1 and itinerant (e_g) electrons with magnetic moment μ_e. In the absence of interactions between them, the corresponding susceptibilities are: (i) a T-dependent Curie susceptibility $\chi_1^0 = C_1/T$ for the μ_1 sublattice with $C_1 = C_{Mn^{4+}} = 1.9\ cm^3\ K\ mol^{-1}$ and (ii) a constant Pauli-like susceptibility χ_e^0 for μ_e. When the interactions between the two sublattices are taken into account in a mean-field approximation, a CW susceptibility is observed as discussed in [26] for Sr_2FeMoO_6. Following that paper, the total susceptibility $\chi(T)$ is:

$$\chi(T) = \chi_e^0 + \frac{C}{(T - \Theta)} \quad (1)$$

where

$$C = C_1(1 + \chi_e^0\lambda_{el})^2 \quad (2)$$

$$\Theta = C_1(\chi_e^0\lambda_{el}^2 + \lambda_{ll}) \quad (3)$$

with λ_{el} and λ_{ll}, the mean-field parameters related to the respective exchange constants.

In this picture, the enhancement of the Curie constant is provided by the FM exchange coupling of the Mn^{4+} through the itinerant electrons (see equation (2)). Considering that, in equation (1), χ_e^0 is usually much smaller than the CW contribution, $C \approx C_{HT}$ provides a reasonable zeroth-order estimation for the enhancement factor $(1 + \chi_e^0\lambda_{el})$.

In order to determine separately the parameters of the model, we may first subtract the AFM superexchange contribution expected (Goodenough–Kanamori rules) between Mn^{4+} ions. An estimation for λ_{ll} may be derived from the Θ value reported [27] for the parent compound $CaMnO_3$, where all the Mn ions are in the tetravalent state, Mn^{4+} ($t_{2g}^3e_g^0$), and no itinerant electrons are present i.e. $\chi_e^0 = 0$ in equation (1). Since the superexchange is very sensitive to the distance between magnetic centres ($J \propto r^{-10}$) and to the angle $\varphi = Mn{-}\widehat{O}{-}Mn$ ($J \propto \cos^2\varphi$) we have taken into account the experimental crystallographic values reported for the whole series $Y_{1-x}Ca_xMnO_3$ in [17]. Therefore we have estimated an approximate ratio $\lambda_{ll}(x = 1)/\lambda_{ll}(x = 0.5) \simeq 2$, obtaining $\lambda_{ll}(x = 0.5) \simeq -94\ mol\ cm^{-3}$. Using this value in equations (1)–(3), self-consistency is obtained for $C = 3.0\ cm^3\ K\ mol^{-1}$, $\Theta = 130\ K$, $\chi_e^0 = 4 \times 10^{-4}\ cm^3\ mol^{-1}$, and $\lambda_{el} = 625\ mol\ cm^{-3}$.

Thus, above 500 K the CW behaviour of the metallic PM phase corresponds to an FM double-exchange mechanism with an enhanced Curie-constant ($C/C_1 = 1.54$). The observed CW-temperature has two contributions: $\Theta_{FM} = C_1\chi_e^0\lambda_{el}^2 \cong 310\ K$, arising from the double-exchange coupling between t_{2g}^3 cores mediated by e_g itinerant electrons, and $\Theta_{AFM} = C_1\lambda_{ll} = -180\ K$, estimated for the superexchange coupling between the t_{2g}^3 cores.

For temperatures below 500 K, $\chi^{-1}(T)$ progressively departs from the high temperature CW behaviour (see figure 2) down to 300 K, where the changes become more pronounced. We may correlate this behaviour with the structural evolution shown in figure 1. This kind of structural variation in other manganites has been associated with localization of the itinerant electrons [2, 28, 29]. The curvature change in $\chi^{-1}(T)$ and, as will be discussed in the next section, a relative maximum in the ESR intensity observed at $T_{CL} = 300\ K$ (see inset in figure 2) is consistent with this charge localization (CL) process.

Between 100 and 200 K, see figure 3, a new Curie–Weiss regime is reached where the high temperature FM interactions are significantly reduced and the effective low temperature Curie constant becomes even larger than in the high-T regime: $C_{LT} \simeq 3.9(1)\ cm^3\ K\ mol^{-1}$, which corresponds to $\mu_{eff} = 5.58\ \mu_B$. This kind of behaviour is qualitatively similar to the case of other doped manganites [3] where an alternative description based on dimer formation, called Zener polarons (ZP), has been proposed as the driving mechanism for charge
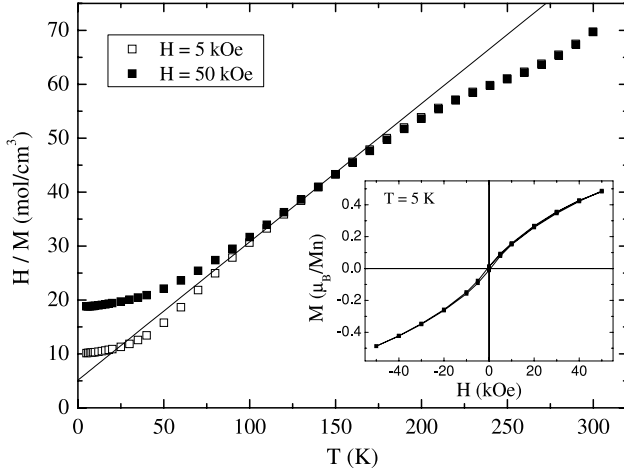
Figure 3. Symbols: H/M versus T taken at two different values of H. Line: low temperature Curie–Weiss fitting. Inset M versus H at $T = 5$ K.

localization. In the ZP model, each e_g electron is trapped between two Mn^{4+} ions. The delocalization of the e_g electron inside the dimer, favoured by the structural distortions, strongly couples ferromagnetically the two Mn^{4+} ions giving a total spin $S_{ZP} = 7/2$. Taking into account that two Mn sites are necessary for each ZP $\mu_{eff} = 5.61\ \mu_B$, the corresponding Curie constant would be $C_{ZP} = 3.94\ cm^3\ K\ mol^{-1}$, in excellent agreement with our experimental C_{LT}.

Finally, below $T \approx 100$ K, the magnetization is no longer lineal with the applied field (see figure 3) indicating some degree of magnetic order, although long range ordering is never achieved [18].

4. Electron spin resonance

In figure 4 we show representative $Y_{0.5}Ca_{0.5}MnO_3$ ESR spectra taken at different T. The resonance consists of a single (without structures) line for all measured temperatures. At high temperatures the line is slightly asymmetrical. Since the magnitude of the linewidth (ΔH) is comparable to the resonance field (H_r), especially at low temperatures, the spectra were processed as indicated in [21] considering a Lorentzian lineshape; the derived parameters ΔH and H_r as a function of T are shown in figure 5. The linewidth decreases slowly with decreasing temperatures down to $T \approx T_{CL}$; below this temperature, ΔH increases and reaches a relative maximum around $T \cong 160$ K with $\Delta H \simeq 3600$ Oe. Below 100 K, ΔH increases again although more rapidly. The resonance field is constant for $T \geq 160$ K and corresponds to a $g = 1.986(4)$. Below 150 K, H_r decreases continuously down to ≈ 1500 Oe at 30 K.

The line intensity, I_{ESR}, is shown in the inset of figure 2. Coincidence between the $I_{ESR}(T)$ and $\chi(T)$ down to temperatures close to T_{CL} is observed when I_{ESR} is normalized to the measured dc high temperature susceptibility. Therefore the same high temperature picture, based on the strong FM interaction of the localized μ_l and the itinerant μ_e magnetic moments, may be considered in
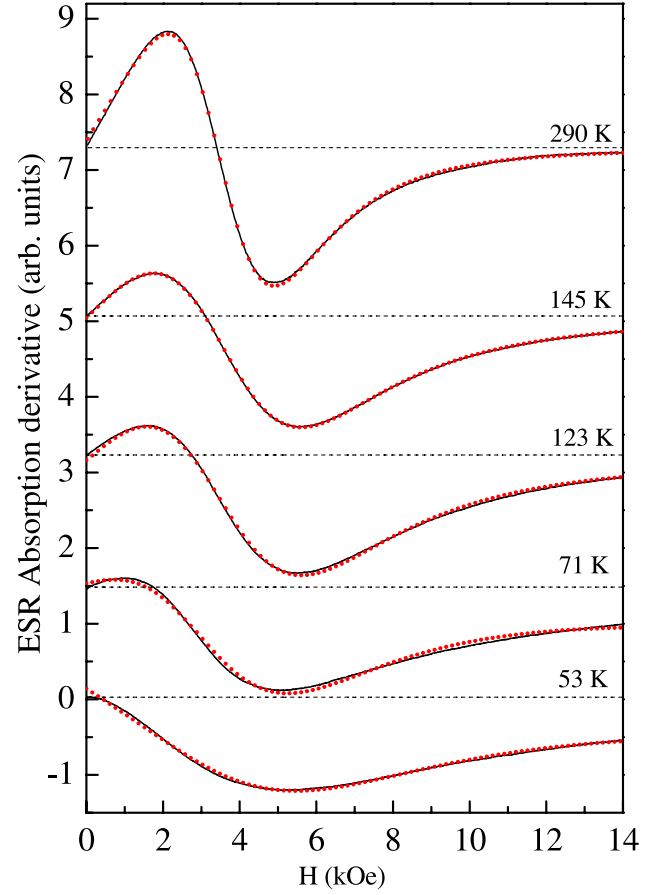
Figure 4. Electron spin resonance spectra measured at the indicated temperatures, the corresponding fitting curves are presented as dotted lines. The curves are vertically shifted for clarity.
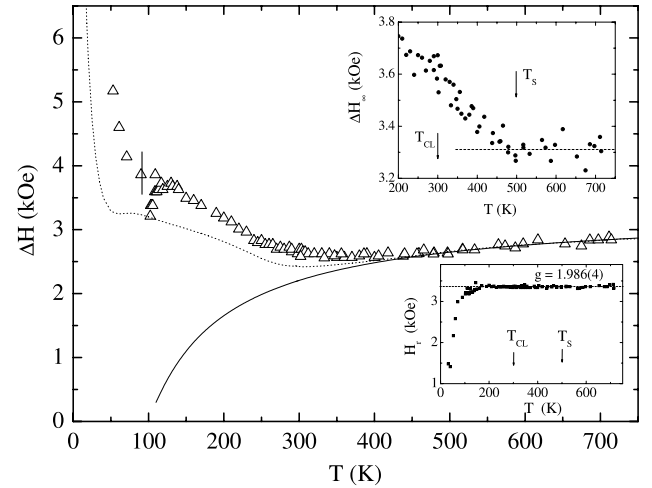
Figure 5. Triangles: temperature dependence of the linewidth, ΔH. Dotted and continuous lines show the fitting to equations (6) and (7). Insets: $H_r(T)$ versus T, the constant value at high temperatures corresponds to a g-factor of 1.986(4); ΔH_∞ versus T showing increasing values for $T < T_{CL}$.

order to describe the $I_{ESR}(T)$ dependence. The spin dynamics of this coupled system is usually taken into account by the Bloch and Hasegawa equations [20]. As in the case

of Sr_2FeMoO_6 [26], where well localized Fe^{3+} moments interact with delocalized electrons, we may associate here a magnetization $\vec{M}_l$ with the Mn^{4+} (t_{2g}^3) cores and $\vec{M}_e$ with the e_g itinerant electrons. The solutions of the Bloch and Hasegawa equations present two well differentiated regimes: bottlenecked and non-bottlenecked, depending of the relative importance of the coupling interactions. In the non-bottlenecked limit both magnetizations tend to respond independently and two resonances may be observed, with their own gyromagnetic factors (g_l and g_e for cores and itinerant electrons, respectively) and linewidths. The single line detected in our experiments suggests [26] the radiofrequency response of an effective magnetization $M = M_l/g_l + M_e/g_e$ in a bottlenecked regime related to the strong M_l–M_e coupling. In this case, the resonance is expected to be centred on an average g-value:

$$g = g_e \frac{\chi_e(T)}{\chi(T)} + g_l \frac{\chi_l(T)}{\chi(T)}. \tag{4}$$

As $g_e \approx g_l$ [30] the average g results are nearly constant at high temperature, in agreement with the data presented in the inset of figure 5.

The linewidth involves two lattice relaxation mechanisms characterized by the individual relaxation times τ_l and τ_e of the localized and itinerant spins, giving [20, 26]:

$$\Delta H(T) = \frac{2}{\sqrt{3}} \left(\frac{\chi_e^0}{\chi(T)} \frac{1}{\gamma \tau_e} + \frac{C_l/T}{\chi(T)} \frac{1}{\gamma \tau_l} \right). \tag{5}$$

Since in our case χ_e^0 is significantly smaller than C_l/T, the behaviour of the coupled system is mainly determined by τ_l and

$$\Delta H(T) \cong \frac{2}{\sqrt{3}} \frac{C_l/T}{\chi(T)} \frac{1}{\gamma \tau_l}. \tag{6}$$

In the high temperature limit, where $\chi(T) \simeq C_{HT}/(T - \Theta_{HT})$, we may rewrite equation (5) in terms of experimental parameters

$$\Delta H(T) = \left(1 - \frac{\Theta_{HT}}{T} \right) \Delta H_\infty. \tag{7}$$

Here $\Delta H_\infty = (C_l/C_{HT})(2/\sqrt{3})(1/\gamma \tau_l)$ is the $\Delta H(T)$ limit value for $T \to \infty$.

From a fitting of the experimental data to equation (7) for $T > 500$ K (see the continuous line in figure 5) we extrapolate $\Delta H_\infty = 3310(40)$ Oe. With this value for ΔH_∞, we may now recalculate the linewidth with equation (6) rewritten as

$$\Delta H(T) = \Delta H_\infty \frac{C_{HT}}{T \chi(T)} \tag{8}$$

using the experimental data for $\chi(T)$. The results (dotted line in figure 5) make a qualitative improvement since they reproduce the minimum around T_{CL}, due to the departure of $\chi(T)$ from the high T Curie–Weiss behaviour.

The reasonable description of $\Delta H(T)$ in a broad temperature range with equation (8) suggests that τ_l is approximately independent of T. According to Anderson and Weiss [31] $1/\gamma \tau_l \propto E_a^2/J$, where anisotropic ($E_a$) and

isotropic (J) interactions are the mechanisms that control, respectively, the broadening and narrowing of the ESR lines. Thus, ΔH_∞ may provide an insight into the nature of these interactions along the series $Y_{1-x}Ca_xMnO_3$. In the case of $CaMnO_3$, a $\Delta H_\infty = 1050(30)$ Oe value was reported in [27, 32]. Taking into account the variation of the exchange interaction discussed in the previous section: $J(x = 1) \approx 2 J(x = 0.5)$, the ratio $\Delta H_\infty(x = 1)/\Delta H_\infty(x = 0.5)$ suggests that $E_a(x = 0.5) \approx 1.3 E_a(x = 1)$. This increase reflects the enhancement of the anisotropic interactions with the lattice distortions [32] that occur with the substitution of Ca by Y [28, 29].

The remaining quantitative differences between predicted and experimental $\Delta H(T)$ may result from minor variations of ΔH_∞ following the structural changes discussed in section 2. The values of ΔH_∞ needed in order to reproduce the experimental data are shown as an inset in figure 5. The increase of ΔH_∞ below $\sim$500 K estimated in this way, is in accordance with the progressive distortion of the lattice in this temperature range, on passing from the O-phase (high T) to the less symmetrical O′ phase (low T).

In the case of the half-doped manganite $YBaMn_2O_6$, a linear high temperature behaviour for $\Delta H(T)$ was interpreted in terms of a Korringa model [33]. This kind of behaviour, mimicking the Korringa-rate, was also predicted by Barnes [20] if $\chi(T)$ can be approximated in equation (5) by a Curie-like C/T law. In our case, this pseudo-linear regime is a reasonable approximation for $\Delta H(T)$ only above 500 K (see figure 5) and the approximation given by equations (6) and (7) applies in a larger range of temperatures. On the other hand, if equations (5)–(8) were used to analyse the $YBaMn_2O_6$ data, a narrower value ($\approx$2000 Oe) will be obtained for ΔH_∞. This result is consistent with the less distorted structure found for the $YBaMn_2O_6$ compound.

At this point we should pay attention to the relative maximum of the I_{ESR} at $T_{CL} \cong 300$ K. Although the static susceptibility, $\chi(T)$, also presents a small anomaly, the variation of $I_{ESR}(T)$ is much more pronounced (see figure 2) and I_{ESR} is significantly reduced relative to $\chi(T)$ below T_{CL}. This behaviour of I_{ESR}, together with the rapid increase of the crystalline distortions (see figure 1), is a clear signal of a progressive localization of the e_g electrons. Notice that resistivity measurements [18] indicate a thermally activated mechanism, $\rho(T) \propto e^{W/k_BT}$, with $W/k_B \approx 1800$ K. For $T \sim T_{CL}$, $W/k_BT \sim 6$ and with this value the hopping of the electrons should be substantially reduced.

Close to 150 K, the ZP formation is responsible for the observed high effective moment and I_{ESR} again approaches $\chi(T)$. Reduction of the ESR intensity in the interphase between delocalized and localized e_g electrons has also been reported in other manganites [13] and would be related to the way in which the different magnetic species interact with each other and their response to the radiofrequency excitations.

5. Discussion

Our experiments clearly reflect the competition between the ferromagnetic effects of the double-exchange mechanism

mediated by e_g electrons and the superexchange antiferromagnetic interaction between the t_{2g}^3 cores. This scenario has been modelled [7] with the ferromagnetic Kondo lattice Hamiltonian that includes a hopping term for the e_g electrons, the Hund's rule coupling, J_H, between them and the localized t_{2g}^3 cores, and the AFM coupling between these cores. A Monte-Carlo calculation of the magnetic phase diagram in the limit of large J_H predicts a metallic ground state when the AFM coupling is relatively weak [7] or the T of the system is sufficiently high [16]. Indeed, our high T picture describes the e_g electrons as fully itinerant, based on the fact that the electrical conductivity is metallic [18], $\rho(500 \text{ K}) = 0.05$ Ω cm. The FM coupling is also reflected in the enhancement of the Curie constant and in the FM character of the Curie–Weiss temperature (see equations (2) and (3)).

As the temperature is lowered, resistivity measurements [18, 29] have shown that thermally activated mechanisms are present in doped manganites, reflecting the hopping of small polarons formed by the e_g electrons and the associated local distortions. Huber *et al* [34] have pointed out that the T dependence of both the susceptibility and the ESR intensity, which mainly follows the paramagnetic behaviour of the t_{2g}^3 cores, is strongly influenced by this hopping of the e_g electrons. Although no microscopic description is yet available, it becomes clear that the behaviour of the coupled system may be expected to be fundamentally different from that of magnetic materials with dominant superexchange interactions [34].

Sometimes, when the hopping is severely restricted, the e_g electrons have been assumed to become totally localized and complete charge ordering has been observed in half-doped manganites [2]. In other cases, formation of FM polarons produced by the alignment of a few neighbouring t_{2g}^3 spins through the hopping of the e_g electron has been proposed to explain experimental results in $Y_{1-x}Ca_xMnO_3$ with $x > 0.75$ [35, 36]. In this direction, Aliaga [16] has shown that the ferromagnetic Kondo lattice model predicts that the system may evolve as a function of decreasing T from a homogeneous PM state with FM short range correlations to a phase where the e_g electrons are 'condensed' in magnetic polarons.

Of special interest are the cases where the filling of the structure with e_g electrons is commensurate with the lattice ($x = 1/2, 1/3, 1/4, \ldots$); maximum gain of kinetic energy is obtained with a small cost in magnetic energy through the formation of FM islands. These polarons show spin and charge correlation functions consistent with the formation of four-, three-, or two-site spin islands containing one e_g electron each [8]. These types of islands have been identified experimentally as two-Mn ZP in $Pr_{0.6}Ca_{0.4}MnO_{0.3}$ [3]. Four-Mn ZP with two e_g in each ZP have been suggested in the case of $YBaMn_2O_6$ [12].

We have interpreted the observed change of the Curie constant in our experiments below 200 K as the formation of magnetic units of this kind, giving rise to a new low T paramagnetic regime. In order to analyse the conditions for the formation of these islands we have performed a mean-field calculation considering a simple lattice of t_{2g}^3 ions with AFM interactions between them. Since the refinement
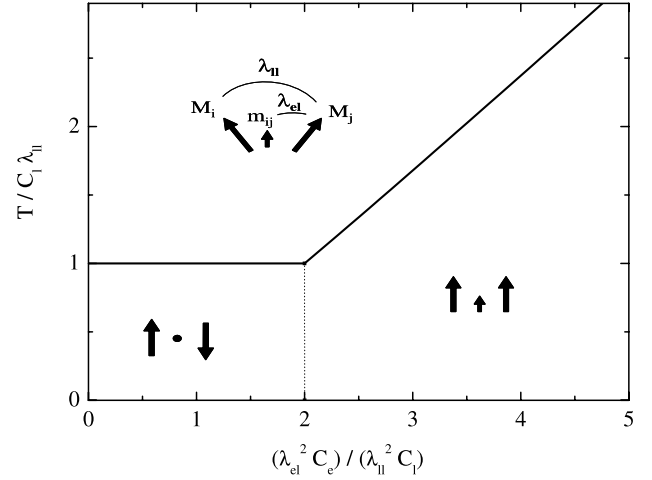
Figure 6. The dimer phase diagram of T versus λ_{el}^2 normalized to a fixed value for λ_{ll}. Solid lines: transition temperatures given by equations (12) or (13) for λ_{el}^2 smaller or larger than $2\lambda_{ll}^2 C_l/C_e$, respectively. Freehand drawings: high and low temperature spin configurations as described in the text.

of the crystal structure of $Pr_{0.6}Ca_{0.4}MnO_3$ has shown a pattern of atom displacements that suggests a dimerization of Mn_1–Mn_2 ions [3] with the e_g electron hopping within these dimers, two pairs of magnetic sublattices were considered $(\mathbf{M}_1, \mathbf{M}_2)$ and $(\mathbf{M}_3, \mathbf{M}_4)$. Each pair represents a dimer, as schematized in figure 2 of [3]. Within each dimer both the AFM superexchange and FM double-exchange interactions are present. The last one is mediated by e_g electrons ($\mathbf{m}_{12}$ and $\mathbf{m}_{34}$). Between dimers only the AFM interaction is assumed to be effective.

The equations for $\mathbf{M}_1$, $\mathbf{M}_2$, and $\mathbf{m}_{12}$ are:

$$\overrightarrow{\mathbf{M}}_1 = \chi_l^0(T)(\overrightarrow{\mathbf{H}} + \lambda_{el}\overrightarrow{\mathbf{m}}_{12} + \lambda_{ll}\overrightarrow{\mathbf{M}}_2 + \lambda_{ll}^*\overrightarrow{\mathbf{M}}_4) \quad (9)$$

$$\overrightarrow{\mathbf{M}}_2 = \chi_l^0(T)(\overrightarrow{\mathbf{H}} + \lambda_{el}\overrightarrow{\mathbf{m}}_{12} + \lambda_{ll}\overrightarrow{\mathbf{M}}_1 + \lambda_{ll}^*\overrightarrow{\mathbf{M}}_3) \quad (10)$$

$$\overrightarrow{\mathbf{m}}_{12} = \chi_e^0(T)(\overrightarrow{\mathbf{H}} + \lambda_{el}(\overrightarrow{\mathbf{M}}_1 + \overrightarrow{\mathbf{M}}_2)) \quad (11)$$

and similar equations for $\overrightarrow{\mathbf{M}}_3$, $\overrightarrow{\mathbf{M}}_4$, and $\overrightarrow{\mathbf{m}}_{3,4}$. The susceptibility $\chi_l^0(T) = C_l/T$, as in section 3. However, for the susceptibility of the e_g electron being no longer itinerant, we assume a Curie behaviour, $\chi_e^0 = C_e/T$. At variance with the treatment in section 3, we allow different AFM coupling parameters within the dimer and between dimers, λ_{ll} and λ_{ll}^*, respectively.

In the absence of an applied field, critical temperatures may be found for non-trivial solutions of an isolated pair ($\lambda_{ll}^* = 0$). AFM order of $\overrightarrow{\mathbf{M}}_1$ and $\overrightarrow{\mathbf{M}}_2$, with the e_g electrons still paramagnetic ($\overrightarrow{\mathbf{m}}_{12} = 0$), is possible for small λ_{el} below a temperature:

$$T_N = C_l|\lambda_{ll}|. \quad (12)$$

Instead, as shown in figure 6, for a double-exchange coupling $\lambda_{el} \geq |\lambda_{ll}|(\sqrt{2C_l/C_e})$, the dimer becomes an FM cluster below T_C, where

$$T_C = -\frac{C_l|\lambda_{ll}|}{2} + \left(\sqrt{\frac{C_l^2|\lambda_{ll}|^2}{4} + C_l C_e \lambda_{el}^2}\right). \quad (13)$$

If the coupling between dimers is $\lambda_{ll}^* \neq 0$ then the ordering temperature is reduced, but the qualitative behaviour remains the same. This seems to be the scenario observed experimentally for $100\,\text{K} \leq T \leq 200\,\text{K}$ in our experiments; a new PM regime is established, compatible with the formation of small FM islands (or Zener polarons) along a wide temperature interval.

At the lowest temperatures, $T \lesssim 75\,\text{K}$, a nonlinear behaviour of $M(H)$ is observed, showing a tendency to saturation that increases with decreasing T as shown in figure 3. For $T \lesssim 25\,\text{K}$, $M(T)$ is almost constant: $M(50\,\text{kOe}, T) \sim 0.5\,\mu_\text{B}$, see inset of figure 3. This complex scenario suggests the appearance of AFM interactions between the dimers, although no clear indication of long range magnetic order was found.

In summary we have described the magnetic behaviour of distorted half-doped manganite in a large temperature range. The magnetization and ESR results are consistent with a picture where the Mn^{4+} are localized and the e_g electrons present an itinerant behaviour at the highest temperature. Close to $T_\text{S} \approx 500\,\text{K}$ a progressive localization of the e_g electrons takes place, favoured by the structural distortion. This localization process settles down at around 200 K where the ZP formation is developed. Interaction between the ZP is observed at lower temperature, although a long range magnetic order is never reached. This description is supported by mean-field calculations which allow us to understand the evolution of the magnetic and ESR parameter of different perovskites as a function of their structural distortion.

Acknowledgments

References

[1] Goodenough J B 1955 *Phys. Rev.* **100** 564 (and references therein)
[2] Rivadulla F, Winkler E, Zhou J-S and Goodenough J B 2002 *Phys. Rev.* B **66** 174432
[3] Daoud-Aladine A, Rodríguez-Carvajal J, Pinsard-Gaudart L, Fernández-Díaz M T and Revcolevschi A 2002 *Phys. Rev. Lett.* **89** 097205
[4] Goff R J and Attfield J P 2004 *Phys. Rev.* B **70** 140404
[5] Rodriguez E E, Proffen Th, Llobet A and Rhyne J J 2005 *Phys. Rev.* B **71** 104430
[6] Giovanetti G, Kumar S, van den Brink J and Picozzi S 2009 *Phys. Rev. Lett.* **103** 037601
[7] Aliaga H, Normand B, Hallberg K, Avignon M and Alascio B 2001 *Phys. Rev.* B **64** 024422
[8] García D J, Hallberg K, Batista C D, Avignon M and Alascio B 2000 *Phys. Rev. Lett.* **85** 3720
[9] García-Fernández M, Staub U, Bodenthin Y, Scagnoli V, Pomjakushin V, Lovesey S W, Mirone A, Herrero-Martín J, Piamonteze C and Pomjakushina E 2009 *Phys. Rev. Lett.* **103** 097205
[10] Lopes A M L, Araújo J P, Amaral V S, Correia J G, Tomioka Y and Tokura Y 2008 *Phys. Rev. Lett.* **100** 155702
[11] Yakubovskii A, Trokiner A, Verkhovskii S, Geashenko A and Khomskii D 2003 *Phys. Rev.* B **67** 064414
[12] Daoud-Aladine A, Perca C, Pinsard-Gaudart L and Rodríguez-Carvajal J 2008 *Phys. Rev. Lett.* **101** 166404 (and references therein)
[13] Zakharov D V, Deisenhofer J, Krug von Nidda H-A, Loidl A, Nakajima T and Ueda Y 2008 *Phys. Rev.* B **78** 235105
[14] Jirák Z, Hejtmánek J, Knížmek K, Krupička S and Maryško M 2004 *J. Magn. Magn. Mater.* **272–276** e1029–30
[15] Nakajima T, Kageyama H, Ichihara M, Ohoyama K, Yoshizawa H and Ueda Y 2004 *J. Solid State Chem.* **177** 987
[16] Aliaga H 2002 *PhD Thesis* Insituto Balseiro
[17] Vega D, Polla G, Leyva A G, Konig P, Lanza H, Esteban A, Aliaga H, Causa M T, Tovar M and Alascio B 2001 *J. Solid State Chem.* **156** 458
[18] Causa M T, Aliaga H, Vega D, Tovar M, Alascio B, Salva H R and Winkler E 2004 *J. Magn. Magn. Mater.* **272–276** 81
[19] Pake G E 1962 *Paramagnetic Resonance* (New York: Benjamin)
[20] Barnes S E 1981 *Adv. Phys.* **30** 801
[21] Causa M T and Passeggi M C G 1983 *Phys. Lett.* A **98** 291
[22] Samuel Smart J 1966 *Effective Field Theories of Magnetism* (Philadelphia: Saunders)
[23] Néel L 1948 *Ann. Phys. (Paris)* **3** 137
[24] Aliaga H, Causa M T, Tovar M, Butera A, Alascio B, Vega D, Leyva G, Polla G and König P 2003 *J. Phys.: Condens. Matter* **15** 249
[25] Tobía D, Vargas J, Winkler E, Vega D, Leyva G, Polla G, Tovar M and Causa M T 2006 *Physica* B **384** 41
[26] Tovar M, Causa M T, Butera A, Navarro J, Martínez B and Fontcuberta J 2002 *Phys. Rev.* B **66** 024409
[27] Huber D L, Alejandro G, Caneiro A, Causa M T, Prado F, Tovar M and Oseroff S B 1999 *Phys. Rev.* B **60** 12155
[28] Vega D, Ramos C, Aliaga H, Causa M T, Alascio B, Tovar M, Polla G, Leyva G, König P and Torriani I 2002 *Physica* B **320** 37
[29] Aliaga H, Causa M T, Alascio B, Salva H, Tovar M, Vega D, Polla G, Leyva G and Konig P 2001 *J. Magn. Magn. Mater.* **226–230** 791
[30] Abragam A and Bleaney B 1970 *Electron Paramagnetic Resonance of Transition Ions* (Oxford: Clarendon)
[31] Anderson P W and Weiss P R 1953 *Rev. Mod. Phys.* **25** 269
[32] Tovar M, Alejandro G, Butera A, Caneiro A, Causa M T, Prado F and Sánchez R 1999 *Phys. Rev.* B **60** 10199
[33] Schaile S, Krug von Nidda H-A, Deisenhofer J, Loidl Af, Nakajima T and Ueda Y 2012 *Phys. Rev.* B **85** 205121
[34] Huber D L, Causa M T, Laura-Ccahuana D and Tovar M 2007 *J. Magn. Magn. Mater.* **310** e604–6
[35] Aliaga H, Causa M T, Salva H, Tovar M, Butera A, Alascio B, Vega D, Polla G, Leyva G and Konig P 2001 arXiv:cond-mat/0010295v5
[36] Aliaga H, Causa M T, Tovar M and Alascio B 2002 *Physica* B **320** 75